IRis

Northeastern University

Physics Faculty Publications

Department of Physics

April 09, 2004

Special photon energies for extracting the bosonic spectral function mediating superconductivity in $Bi_2Sr_2CaCu_2O_8$ via angle-resolved photoemission spectroscopy

M. Lindroos
Northeastern University

R. S. Markiewicz
Northeastern University

A. Bansil
Northeastern University

Recommended Citation

Lindroos, M.; Markiewicz, R. S.; and Bansil, A., "Special photon energies for extracting the bosonic spectral function mediating superconductivity in $Bi_2Sr_2CaCu_2O_8$ via angle-resolved photoemission spectroscopy" (2004). *Physics Faculty Publications.* Paper 428.

This work is available open access, hosted by Northeastern University.

PHYSICAL REVIEW B **69**, 140505(R) (2004)

Special photon energies for extracting the bosonic spectral function mediating superconductivity in $Bi_2Sr_2CaCu_2O_8$ via angle-resolved photoemission spectroscopy

M. Lindroos,[1,2] R. S. Markiewicz,[1] and A. Bansil[1]
[1]*Physics Department, Northeastern University, Boston, Massachusetts 02115, USA*
[2]*Tampere University of Technology, P.O. Box 692, FIN-33101 Tampere, Finland*
(Received 4 November 2003; published 9 April 2004)

We delineate the complex nature of the angle-resolved photoemission spectroscopy (ARPES) matrix element in $Bi_2Sr_2CaCu_2O_8$ and identify photon energies where the matrix element is insensitive to wave vector and/or frequency. These special photon energies provide a unique route for extracting the spectral function of the bosonic glue mediating superconductivity and for obtaining self-energies more generally via ARPES experiments.

DOI: 10.1103/PhysRevB.69.140505 PACS number(s): 74.72.−h, 71.15.Ap, 71.18.+y, 74.20.Mn

Recently, Vekhter and Varma[1] have proposed a scheme for extracting the spectral function $A_{glue}(k,\omega)$ of the bosonic glue mediating superconductivity in the cuprates via angle-resolved photoemission spectroscopy (ARPES) experiments. The idea is to solve the Eliashberg equation self-consistently for A_{glue} using the measured photointensity data. A key assumption necessary for implementing this procedure is that the ARPES matrix element (ME) depends weakly on wave vector $k_\parallel$, initial state energy ω, and temperature T.[2] Unfortunately, however, ME effects are known to be strong:[3–8] the ME generally varies by orders of magnitude with $k_\parallel$ as one goes around the Fermi surface (FS) and by several hundred percent with ω for the energy scale over which the bosonic glue will be expected to mix with initial states. In this paper, we present a unique route for circumventing this dilemma by exploiting the photon energy dependence[9–12] of the ME.

We have carried out extensive simulations of the ARPES photointensity throughout the Brillouin zone (BZ) for exciting states from the bonding as well as the antibonding FS in $Bi_2Sr_2CaCu_2O_8$ (Bi2212) for a wide range of photon energies $h\nu$. The binding-energy range considered is ~ 3 times the superconducting energy scale, which should be adequate for treating the mixing of the bosonic glue. The constancy of the ME is analyzed in terms of a simple measure of variations defined by variance as a percentage of the normalized average intensity. A precise definition of how much the ME varies at a given $h\nu$ with $k_\parallel$ and/or ω then follows. The presented results allow us to obtain the specific $h\nu$'s where the ME remains constant within a particular level of tolerance and to determine how different regions of the $(k_\parallel,\omega)$ space contribute in this regard. Photon energies, where the ME displays a weak $k_\parallel$ and ω dependence, provide special windows for applying schemes such as those of Ref. 1, and for investigating self-energy effects more generally via ARPES (e.g., the kink physics).

All computations in this paper have been carried out within the one-step methodology, which we have generalized to treat arbitrarily complex unit-cell materials.[3,13,14] The photointensity is thus modeled realistically in the presence of a specific surface termination—taken here to be in the BiO layer. The effects of multiple scattering and the ARPES matrix element are thus included. The crystal potential was obtained for Bi2212 through a self-consistent Korringa-Kohn-Rostoker band-structure scheme assuming a perfect tetragonal lattice.[13] The actual potential was modified somewhat to lift the BiO pockets around the $(\pi,0)$-point above the Fermi energy E_F to account for their absence in the ARPES spectra. Otherwise, our band structure and FS are in accord with the well-known results in Bi2212. The finite lifetimes of the initial and final states are incorporated by introducing suitable imaginary parts to the self-energies of the associated propagators. The initial-state width was chosen to be small (14 meV) for ease in distinguishing between closely placed bonding and antibonding states. Similarly, a fixed final-state width of 2 eV was used to accentuate the ME effect. We have however carried out simulations using more complicated energy-dependent lifetimes to establish that our conclusions are insensitive to these details.

Figure 1 gives the total ARPES intensities computed within the one-step model when electrons for various $k_\parallel$ values (specified by the angle θ) are excited from the bonding (left) or the antibonding (right) portions of the FS. $h\nu$ values up to 80 eV are considered. For unpolarized light, the intensity is symmetric around the nodal ($\theta=45°$) direction, and for this reason results are shown only over the $\theta=0°$–$45°$

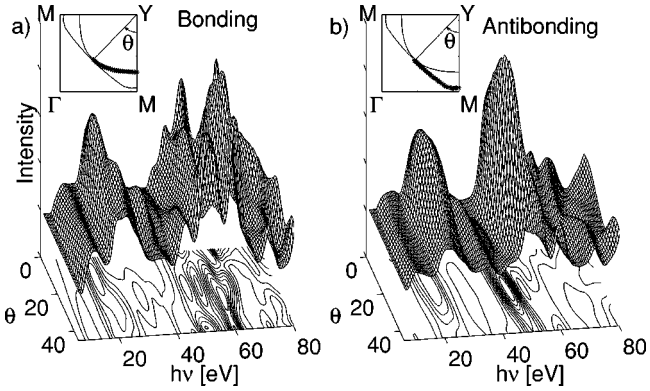

FIG. 1. ARPES intensity for emission from the bonding (left) and antibonding (right) sheets of the FS (highlighted in the insets) in Bi2212 as a function of $k_\parallel$ and $h\nu$ is shown both in a three-dimensional rendition and as a contour plot. $k_\parallel$ values are given in terms of the angle θ along the FS, with $\theta=0°$ denoting the antinodal Y-M direction. Light is assumed unpolarized.

 ©2004 The American Physical Society

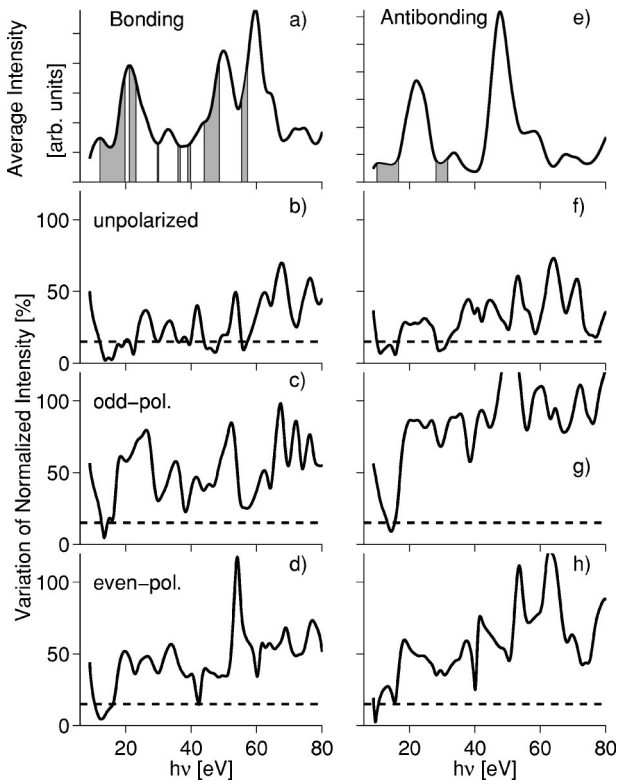

FIG. 2. Variation in ARPES intensity with $k_{\parallel}$ as a function of $h\nu$ for the bonding (left) and antibonding (right) FS's. (a) and (e) give values obtained by averaging over $k_{\parallel}$. The remaining frames give standard deviations as a percentage of the mean for unpolarized as well as "even" and "odd" polarization of light as discussed in the text. Dashed lines identify $h\nu$ regions where the intensity changes with $k_{\parallel}$ are less than $\pm 15\%$, and are marked with gray bands for unpolarized light in (a) and (e).

range. It is evident that in general the intensity or equivalently the ME varies strongly with θ and $h\nu$, although there are $h\nu$ values where the intensities are more or less constant over the whole FS. In contrast, the ME varies strongly as a function of $h\nu$ at any θ.

Figure 2 delineates the sensitivity of the ME to $k_{\parallel}$. For this purpose, we first compute intensities I_i for emission from a mesh of $k_{\parallel}$ points $k_i = k_{\parallel}(\theta_i)$ (spaced uniformly in θ) lying on the bonding or the antibonding FS at a fixed value of $h\nu$. From this (k_i, I_i) set the average intensity $\overline{I}$ and the corresponding standard deviation σ are straightforwardly defined. $\sigma/\overline{I}$ then provides a reasonable measure of the extent to which the ME remains constant as one goes around the FS. Figure 2 displays σ as a percentage of $\overline{I}$. In order to help clarify things, we focus on frame (b) for the bonding FS first. We see that around $h\nu = 13.5$–15.5 eV, the variation is nearly zero, indicating that the ME remains essentially constant over the entire bonding FS in this energy range.[15] On the other hand, for $h\nu = 66$–69 eV, variation is quite large being over $\pm 50\%$. Looking below the $\pm 15\%$ level (dashed line), we can identify several energy ranges where the ME is relatively constant. These energy regions are marked as gray bands in (a), which gives the average intensity $\overline{I}$. Obviously,

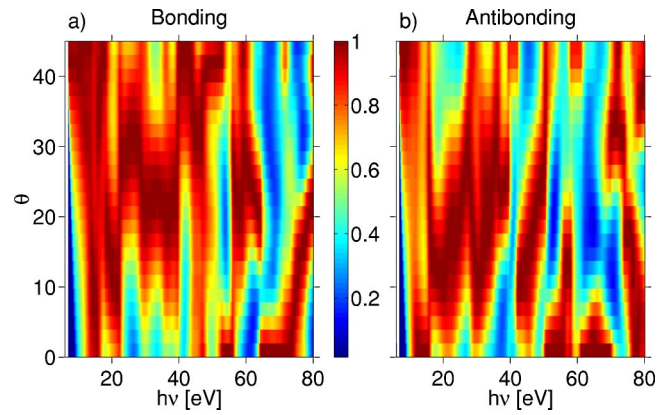

FIG. 3. (Color online) Variations in the intensities of Figs. 2(b) and 2(f) as a function of $k_{\parallel}$ (given by θ as in Fig. 1) for the bonding and the antibonding FS for unpolarized light. Maximum intensity at each $h\nu$ is normalized to unity.

of greatest interest are $h\nu$'s, where not only the ME is nearly constant, but also the cross section for emission is high. The $h\nu$'s where the ME variations display higher or lower tolerance than the $\pm 15\%$ level can be read from (b).

We comment next on other frames of Figs. 2(c) and 2(d) which present the effect of polarization. "Even" refers to the case where the polarization vector lies along the radial direction from the $Y(\pi,\pi)$ point, and "odd" to the case where the polarization is perpendicular to this radial direction. The important point is that the size of variations in (c) or (d) is substantially larger than in (a), so that polarized light is intrinsically less suited for achieving constancy of ME's. The right frames (e)–(h), which refer to the excitation of the antibonding FS, elicit comments similar to those made above for the bonding FS. By comparing (b) and (f), we see however that the ME on the antibonding FS is somewhat more sensitive to $k_{\parallel}$ than the bonding FS.

Figure 2, does not give information on how the ME changes as one moves along the FS or its behavior in the vicinity of the nodal or the antinodal point. Insight in this regard is provided by Fig. 3,[16] which gives the value of the relative intensity as a function of $k_{\parallel}$ on a color scale with the maximum defined as unity at each $h\nu$. Looking at the bonding FS in Figs. 3(a) and 2(b), we see, for instance, that at 60 eV, even though the variation over the whole FS is quite large, most of this variation comes from near the antinodal point ($\theta = 0$), but otherwise the ME remains quite constant over a large arc around the nodal point ($\theta = 45°$). In contrast, at 75 eV the intensity is quite high and uniform around the antinodal point, but is low around the nodal point, while at 35 eV, it is uniformly high, away from both the nodal and the antinodal points. Similar effects can be seen for the antibonding FS in Fig. 3(b).

Figure 4 illustrates how the $k_{\parallel}$ dependency of the ME plays out at two specific photon energies. At 22.4 eV, (a) shows that the FS emission from the bonding band has roughly the same intensity throughout the first BZ (white square), as expected from the low variance at this energy in Fig. 2(b). By contrast, the variance for the antibonding FS is larger [see Fig. 2(f)], but this is due mostly to the intensity

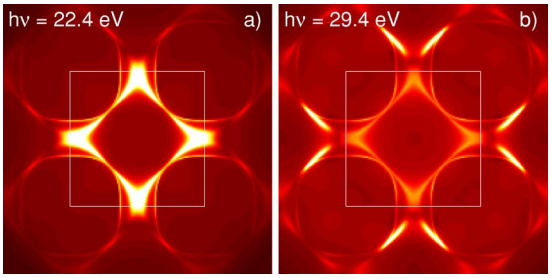

FIG. 4. (Color online) ARPES emission intensity from the FS in Bi2212 for 22.4 eV and 29.4 eV photons (unpolarized). White square marks the first BZ.

being low around the nodal point, which is evident also in Fig. 3(b). At 29.4 eV, on the other hand, *both* the bonding and the antibonding FS's give small variance and Fig. 4(b) indeed shows little change in intensity. Note that outside the first BZ, intensities are far from constant in Fig. 4.[17]

We turn now to discuss the dependence of the ME on initial-state energy (or equivalently the frequency). The measure of variations is the same as that used previously in Fig. 2, except that here we compute the intensity for a $k_{\parallel}$ point on the FS as the associated band disperses below E_F [see Figs. 5(a) and 5(b)]. The binding energies are considered over the scale of the bilayer splitting Δ_{bi} at $(\pi,0)$. Given that the measured values of Δ_{bi} are $\sim$80 meV and the superconducting gap Δ_{su} is $\sim$20–50 meV, depending on doping, Δ_{su} is $\sim$25–60% of Δ_{bi}. Since coupling with any bosonic mode will be expected to mix states over an energy scale of a few times Δ_{su}, the reasonable scale for considering constancy of the ME is Δ_{bi}. Accordingly, Fig. 5 presents results for three $k_{\parallel}$ values on the bonding FS, including the nodal (k_3) and the antinodal points (k_1). The antibonding FS is considered only along the antinodal direction in the interest of brevity.[18]

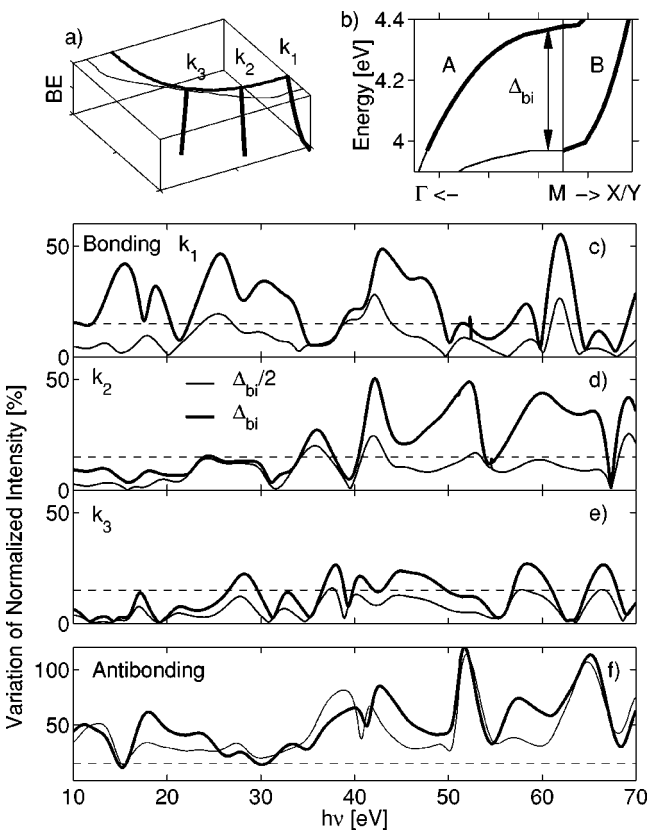

FIG. 5. Variations in ARPES intensity (defined by percentages as in Fig. 2) with binding energy (BE) over energy scales of Δ_{bi} and $\Delta_{bi}/2$, as a function of $h\nu$ for unpolarized light. Dashed lines mark changes at the $\pm 15\%$ level. Results for three $k_{\parallel}$ values k_1, k_2, and k_3 at E_F for the bonding (B) band are shown in (c)–(e), and for one $k_{\parallel}$ value (along the antinodal direction) for the antibonding (A) band in (f). A and B bands are shown in (b). Δ_{bi} is the bilayer splitting at $(\pi,0)$. The FS's and the B band dispersing to lower energies at $k_1 - k_3$ are shown in (a). Note scale change in (f).

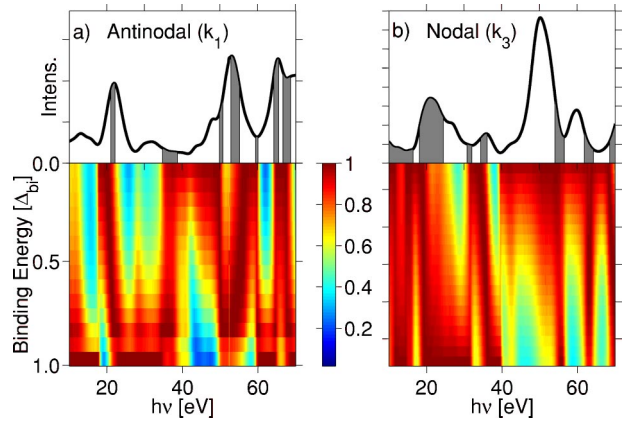

FIG. 6. (Color online) Variations in normalized intensities of Figs. 5(c) and 5(e) as a function of binding energy for the bonding band along the antinodal (left frame) and nodal directions (right frame). Upper frames give average intensity as a function of $h\nu$, where regions of low variation in ME are identified by gray bands.

In looking at Fig. 5, we comment on the bonding (B) band in (c)–(e) first. Over the energy scale of $\Delta_{bi}/2$, variations are generally below the $\pm 15\%$ level throughout the photon energy range, and this continues to be the case for the $k_{\parallel}$ region near the nodal direction in (e) and (d) for photon energies up to $\sim$40 eV, even over the scale of Δ_{bi}. The antinodal direction is quite sensitive to the energy scale as seen by comparing the two curves in (c), although there are energies such as 21, 35–37, 54–55, and 68 eV, where the absolute variance is small. The typical results for the antibonding (A) band, in (f), draw comments similar to those made above for the B band. The variations are however generally larger than for the B band, with the curves in (f) (note scale change) mostly lying above the $\pm 15\%$ line. Figure 6 provides further insight into the energy dependence of the ME. The behavior of the B band is depicted along the antinodal and nodal directions. Energy ranges of low variation are identified with gray bands in the upper frames, together with the total-energy-averaged intensity, where the latter allows one to assess the extent to which a given photon energy is suited for obtaining a reasonable overall ARPES cross section.[19]

In summary, we have delineated the complex nature of the ARPES matrix element in Bi2212 for the purpose of identifying photon energies where the matrix element is insensitive to wave vector $k_{\parallel}$ and/or the initial-state energy ω. For unpolarized light, at the $\pm 15\%$ tolerance level, the dependency

of the matrix element on $k_{\parallel}$ is found to be weak around $h\nu = 12-23$, 30, 36, 39, 44–48, and 55–57 eV for the bonding FS, and around $h\nu = 10-17$ and 28–32 eV for the antibonding FS. The corresponding energies where the ω dependence is weak are 15–16 and 30 eV for the antibonding FS and generally below 35 eV for the bonding FS. Additionally, ω dependence is weak near the *nodal* direction at photon energies around 10–24, 31–36, 54–56, 61–64, and 68–70 eV, and near the *antinodal* direction near 21–22 and 35–38 eV. By relaxing the tolerance with respect to $k_{\parallel}$ and/or ω, other energies can be obtained from the data presented in Figs. 2 and 5, and guidance as to how these variations arise from more limited $k_{\parallel}$ and ω regions in the underlying spectra from Figs. 3 and 6. Such special photon energies would provide a different route for extracting the bosonic spectral function involved in superconductivity via ARPES measurements through proposals such as those of Ref. 1 by circumventing the complications introduced by the $k_{\parallel}$ and ω dependencies of the ARPES matrix element.

This work was supported by the U.S. Department of Energy Contract No. DE-AC03-76SF00098, and benefited from the allocation of supercomputer time at NERSC, Northeastern University's Advanced Scientific Computation Center (ASCC), and the Institute of Advanced Computing (IAC), Tampere.

[1] I. Vekhter and C.M. Varma, Phys. Rev. Lett. **90**, 237003 (2003).

[2] T dependence of the ME should be small, if the system does not undergo any significant structural change.

[3] A. Bansil and M. Lindroos, Phys. Rev. Lett. **83**, 5154 (1999).

[4] M.C. Asensio, J. Avila, L. Roca, A. Tejeda, G.D. Gu, M. Lindroos, R.S. Markiewicz, and A. Bansil, Phys. Rev. B **67**, 014519 (2003).

[5] D.L. Feng, C. Kim, H. Eisaki, D.H. Lu, A. Damascelli, K.M. Shen, F. Ronning, N.P. Armitage, N. Kaneko, M. Greven, J.-i. Shimoyama, K. Kishio, R. Yoshizaki, G.D. Gu, and Z.-X. Shen, Phys. Rev. B **65**, 220501(R) (2002).

[6] A.A. Kordyuk, S.V. Borisenko, T.K. Kim, K.A. Nenkov, M. Knupfer, J. Fink, M.S. Golden, H. Berger, and R. Follath, Phys. Rev. Lett. **89**, 077003 (2002).

[7] A. Damascelli, Z.-X. Shen, and Z. Hussain, Rev. Mod. Phys. **75**, 473 (2003).

[8] J. C. Campuzano, M. R. Norman, and M. Randeria, in *Physics of Conventional and Unconventional Superconductors*, edited by K. H. Bennemann and J. B. Ketterson (Springer-Verlag, Berlin, 2004), Vol. 2.

[9] P.V. Bogdanov, A. Lanzara, X.J. Zhou, S.A. Kellar, D.L. Feng, E.D. Lu, H. Eisaki, J.-I. Shimoyama, K. Kishio, Z. Hussain, and Z.X. Shen, Phys. Rev. B **64**, 180505(R) (2001).

[10] A. Kaminski, S. Rosenkranz, H.M. Fretwell, Z. Li, H. Raffy, M. Randeria, M.R. Norman, and J.C. Campuzano, Phys. Rev. Lett. **90**, 207003 (2003).

[11] Y.-D. Chuang, A. D. Gromko, A. V. Fedorov, Y. Aiura, K. Oka, Y. Ando, M. Lindroos, R. S. Markiewicz, A. Bansil, and D. S. Dessau, Phys. Rev. B **69**, 094515 (2004).

[12] T.K. Kim, A.A. Kordyuk, S.V. Borisenko, A. Koitzsch, M. Knupfer, H. Berger, and J. Fink, Phys. Rev. Lett. **91**, 167002 (2003).

[13] M. Lindroos, S. Sahrakorpi, and A. Bansil, Phys. Rev. B **65**, 054514 (2002).

[14] S. Sahrakorpi, M. Lindroos, and A. Bansil, Phys. Rev. B **68**, 054522 (2003).

[15] The exact energy values depend weakly on the choice of final-state self-energy.

[16] Figure 1 in principle, contains the variation of the ME as one goes around the FS, but this information is difficult to read in the plot. Figure 3 is better suited for this purpose since it considers ME normalized to unity at each photon energy, allowing one to focus on variations and to more easily identify the behavior near the antinodal and nodal points.

[17] Variations considered in Figs. 2 and 3 extend only to the $k_{\parallel}$ region of the first BZ, but should be adequate for most theoretical analyses.

[18] Note that our computation of the ME involves staying on the dispersion curve $\omega = \epsilon_k$. It will be interesting to consider ω dependence outside this constraint, but a procedure for doing so within our first-principles framework is not known. However, the correlated superconducting state is produced by the mixing of bare states over the energy scale Δ_{bi} around the bosonic mode. Therefore, a sampling of bare states over the scale Δ_{bi}, as we have carried out, provides a reasonable measure of the ω dependence of the ME.

[19] The present analysis shows that the lineshape will be complicated by the intrinsic ω dependency of the ARPES matrix element. Therefore, caution should be exercised in addressing the delicate issue of ω dependency of the self-energy in Bi2212 via simple fits to the ARPES lineshapes using Lorentzians to model the bonding and antibonding components.